Contribution from Ames Laboratory and the Department of Chemistry, Iowa State University, Ames, Iowa 50011

Effect of Coordinating Anions on the Kinetics and Thermodynamics of Oxygen Binding by a Macrocyclic Cobalt(II) Complex

Andreja Bakac* and James H. Espenson*

Received September 14, 1989

The macrocyclic cobalt(II) complexes $(X)L^2Co^+$ ($X^- = Cl^-$, SCN^-; L^2 = *C-meso*-5,7,7,12,14,14-hexamethyl-1,4,8,11-tetraazacyclotetradecane) react with O_2 to yield $(X)L^2CoO_2^+$. The kinetics of the forward reaction in aqueous solution at 25 °C ($X^- = Cl^-$, $k = 1.80 \times 10^6$ M^{-1} s^{-1}; $X^- = SCN^-$, $k = 7.29 \times 10^6$ M^{-1} s^{-1}) are similar to those for the unsubstituted, presumably diaquo complex L^2Co^{2+} ($k = 5.00 \times 10^6$ M^{-1} s^{-1}). The dissociation of O_2 from $(X)L^2CoO_2^+$ takes place with the rate constants of 3300 s^{-1} and <500 s^{-1} for the chloro and thiocyanato complexes, respectively. The accelerated autoxidation of L^2Co^{2+} in the presence of Cl^- is attributed to catalysis of the redox steps following oxygen binding. In the case of SCN^- the autoxidation is also promoted by the large equilibrium constant for O_2 binding by $(SCN)L^2Co^+$. The compound $L^2Co(ClO_4)_2$ crystallizes in the monoclinic space group $P2_1/n$ with two molecules in a unit cell of dimensions $a = 8.396$ (1) Å, $b = 9.149$ (1) Å, $c = 15.385$ (2) Å, and $\beta = 97.449$ (6)°. The data refined to a final value of the weighted R factor of 0.0421. The cobalt ion is located at the crystallographic center of inversion, which coincides with the center of the equatorial plane containing the four nitrogens. The two axial positions are occupied by the perchlorates.

Introduction

The reactions of O_2 with metal complexes, such as LCo^{II} (L represents all the ligands bound to the cobalt), often take place according to the two-step scheme of eqs 1 and 2.[1,2] The binuclear

$$LCo^{II} + O_2 \rightarrow LCo^{III}O_2 \quad (1)$$

$$LCo^{III}O_2 + LCo^{II} \rightarrow LCo^{III}O_2Co^{III}L \quad (2)$$

product of eq 2 subsequently decomposes in a less well defined reaction(s). At least some of the steps in the overall reduction of O_2 are catalyzed by halides, thiocyanate, nitrite, and other anions and by H^+.[3,4] However, owing to the complexity of the reactions with O_2, it is difficult to assign an exact role to the anions and H^+ in the overall scheme.[3] It has been established in the earlier work[4] that Cl^- and H^+ catalyze the decomposition of the binuclear adduct $(([14]aneN_4)Co)_2O_2^{4+}$, but the effect of Cl^- on the earlier stages of the reaction of $Co([14]aneN_4)(H_2O)_2^{2+}$ (hereafter L^1Co^{2+}) with O_2 has not been studied.

One might expect that coordinating anions, such as halides, would influence the kinetics of both the forward and reverse reactions of eqs 1 and 2 by stabilizing species containing cobalt in the (formal)[1e,5] 3+ oxidation state. The binding of oxygen to metal complexes is known to be altered by the presence of Lewis bases[1,6,7] either as a result of a change in the coordination number of the metal reactant or because of the effect of the coordinated base on the stability of the metal-oxygen adduct. For example, a cobalt(II) complex of a functionalized cyclam containing an appended imidazole that is axially coordinated to the cobalt forms a 1:1 complex with O_2 at room temperature in aqueous solution.[7] Under identical conditions the cobalt(II) complex of the nonfunctionalized cyclam forms a 2:1 μ-peroxo complex. However, no kinetic data are available in any of the cases mentioned.

We have recently studied the reaction of $Co(C\text{-}meso\text{-}Me_6[14]aneN_4)(H_2O)_2^{2+}$ (hereafter L^2Co^{2+}) with O_2 by laser flash photolysis.[8,9] The reaction proceeds according to eq 1 with no evidence for the formation of a binuclear adduct. It has been noticed that coordinating anions accelerate the overall oxidation of the complex, but it was not known whether the major effect was on reaction 1 or on the subsequent decomposition steps. Since reaction 1 in this system is well separated in time from the decomposition steps, a study of the anion effect on the kinetics of reaction 1 in both directions is feasible. Here we report the results of such a study. Kinetic data were not collected for the parent compound, L^1Co^{2+}, owing to the instability of its solutions containing O_2 and coordinating anions.

We have now also succeeded in obtaining a single crystal of $L^2Co(ClO_4)_2$. The crystal structure of the compound was determined by X-ray diffraction.

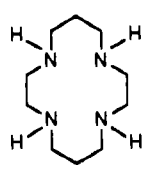

$[14]aneN_4 = L^1$

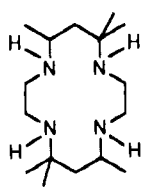

$Me_6[14]aneN_4 = L^2$

Experimental Section

The macrocyclic ligand L^2 and the cobalt(II) complexes L^1Co^{2+} and L^2Co^{2+} were prepared as previously described.[8] NaCl (Mallinckrodt) was recrystallized two times from water. The results obtained with this material were identical with those obtained with the unpurified salt. LiSCN was available from our previous work.[10]

The equilibrium constant for the formation of $(SCN)L^2Co^+$ from L^2Co^{2+} and SCN^- (eq 3) was determined by preparing solutions of L^2Co^{2+} in the presence of a number of different concentrations of SCN^-

$$L^2Co^{2+} + SCN^- \rightleftharpoons (SCN)L^2Co^+ \quad (3)$$

at 0.10 M ionic strength ($LiClO_4$) under strictly anaerobic conditions. The absorbance of these solutions was measured at 490 nm, a maximum in the spectrum of $(SCN)L^2Co^+$. Despite the more favorable absorbance changes associated with reaction 3 in the near-UV region, measurements in that spectral range were avoided owing to the large effects on absorbance of even the minute amounts of oxygen. The data obtained at 490 nm were fitted to eq 4, where $\Delta\epsilon$ represents the difference between the

$$\Delta\epsilon = K_3(\Delta\epsilon_0)[SCN^-]_{eq}/(1 + K[SCN^-]_{eq}) \quad (4)$$

(1) (a) Jones, R. D.; Summerville, D. A.; Basolo, F. *Chem. Rev.* **1979**, *79*, 139. (b) Niederhoffer, E. C.; Timmons, J. H.; Martell, A. E. *Chem. Rev.* **1984**, *84*, 137. (c) Drago, R. S.; Corden, B. B.; Zombeck, A. *Comments Inorg. Chem.* **1981**, *1*, 53. (d) *Oxygen Complexes and Oxygen Activation by Transition Metals*; Martell, A. E., Sawyer, D. T., Eds.; Plenum: New York, 1988. (e) Taube, H. *Prog. Inorg. Chem.* **1986**, *34*, 607.

(2) Chen, D.; Martell, A. E.; Sun, Y. *Inorg. Chem.* **1989**, *28*, 2647 and references therein.

(3) Dreos, R.; Tauzher, G.; Costa, G.; Green, M. *J. Chem. Soc., Dalton Trans.* **1975**, 2329.

(4) (a) Wong, C.-L.; Endicott, J. F. *Inorg. Chem.* **1981**, *20*, 2233. (b) Wong, C.-L.; Switzer, J. A.; Balakrishnan, K. P.; Endicott, J. F. *J. Am. Chem. Soc.* **1980**, *102*, 5511.

(5) (a) Tovrog, B. S.; Kitko, D. J.; Drago, R. S. *J. Am. Chem. Soc.* **1976**, *98*, 5144. (b) Bailey, C. L.; Drago, R. S. *Coord. Chem. Rev.* **1987**, *79*, 321.

(6) McLendon, G.; Mason, M. *Inorg. Chem.* **1978**, *17*, 362.

(7) Kimura, E.; Shionoya, M.; Mita, T.; Iitaka, Y. *J. Chem. Soc., Chem. Commun.* **1987**, 1712.

(8) Bakac, A.; Espenson, J. H. *J. Am. Chem. Soc.* **1990**, *112*, 2273.

(9) The stereochemistry of the coordinated macrocycles has been discussed in detail (Curtis, N. F. In *Coordination Chemistry of Macrocyclic Compounds*; Nelson, G. A., Ed.; Plenum: New York, 1979; Chapter 4). Abbreviations used: $[14]aneN_4$ = 1,4,8,11-tetraazacyclotetradecane; $Me_6[14]aneN_4$ = *C-meso*-5,7,7,12,14,14-hexamethyl-1,4,8,11-tetraazacyclotetradecane.

(10) Bakac, A.; Espenson, J. H.; Miller, L. P. *Inorg. Chem.* **1982**, *21*, 1557.

0020-1669/90/1329-2062$02.50/0 © 1990 American Chemical Society

Table I. Crystallographic Data for [Co(*C-meso*-Me_6[14]aneN_4)(ClO_4)$_2$]

formula	$CoC_{16}H_{36}N_4O_8Cl_2$
fw	542.33
space group	$P2_1/n$ (No. 14)
a, Å	8.396 (1)
b, Å	9.149 (1)
c, Å	15.385 (2)
β, deg	97.449 (6)
V, Å^3	1171.8 (2)
Z	2
d_{calc}, g/cm^3	1.537
cryst size, mm	0.27 × 0.28 × 0.31
μ(Mo Kα), cm^{-1}	10.06
data collcn instrum	Enraf-Nonius CAD4
radiation (monochromated in incident beam)	Mo Kα (λ = 0.71073 Å)
no. of orientation reflcns; range (2θ), deg	25; 18.8–35.3
temp, °C	−20
scan method	ω–2θ
data collcn range, 2θ, deg	4–50
no. of unique data: tot.; with $F_o^2 > 3\sigma(F_o^2)$:	2050; 1573
no. of params refined	142
R^a	0.0304
R_w^b	0.0421
quality-of-fit indicator^c	1.20
largest shift/esd, final cycle	<0.01
largest peak, e/Å^3	0.31 (6)

$^a R = \sum||F_o| - |F_c||/\sum|F_o|$. $^b R_w = [\sum w(|F_o| - |F_c|)^2/\sum w|F_o|^2]^{1/2}$; $w = 1/\sigma^2(|F_o|)$. Neutral-atom scattering factors and anomalous scattering corrections were taken from: *International Tables for X-ray Crystallography*; The Kynoch Press: Birmingham, England, 1974; Vol. IV. ^{c}Quality-of-fit = $[\sum w(|F_o| - |F_c|)^2/(N_{observns} - N_{params})]^{1/2}$.

molar absorptivities of the equilibrated solutions and that of L^2Co^{2+}, $\Delta\epsilon_0$ is the difference between the molar absorptivities of $(SCN)L^2Co^+$ and L^2Co^{2+}, and $[SCN^-]_{eq}$ is the equilibrium concentration of SCN^-. The equilibrium constant was first estimated by using the initial $[SCN^-]$ in eq 4. The values of $[SCN^-]_{eq}$ were then calculated from the initial concentrations and the estimated K_3, and the process was repeated. The data converged to give consistent values of K_3 and $[SCN^-]_{eq}$ in two iterations.

The reaction of L^2Co^{2+} with Cl^- (eq 5) causes no absorbance change in the visible and near-UV parts of the spectrum. The equilibrium

$$L^2Co^{2+} + Cl^- \rightleftharpoons (Cl)L^2Co^+ \qquad (5)$$

constant K_5 was thus determined by a competition method, on the basis of the assumption that eqs 3 and 5 represent the only important equilibria in solutions containing L^2Co^{2+}, Cl^-, and SCN^-. This is a reasonable assumption under the conditions employed, since there was no evidence for the coordination of more than one SCN^- to L^2Co^{2+} in the absence of Cl^-, and the binding of the chloride to L^2Co^{2+} is extremely weak, such that the formation of higher complexes containing either additional Cl^- or SCN^- seems to be ruled out.

The absorbance of solutions containing L^2Co^{2+} and variable amounts of NaCl and LiSCN at 0.5 M ionic strength and 25 °C was measured at 490 nm. The data were fitted to eq 6, where ϵ_{CoNCS}, ϵ_{obs}, and ϵ_1 are

$$\frac{[SCN^-]_{eq}(\epsilon_{CoNCS} - \epsilon_{obs})}{\epsilon_{obs} - \epsilon_1} = (1 + K_5[Cl^-]_{eq})/K_3 \qquad (6)$$

the molar absorptivities of $(SCN)L^2Co^+$ (126 M^{-1} cm^{-1}; see later), of equilibrated solutions, and of L^2Co^{2+} (67.8 M^{-1} cm^{-1}), respectively. The ϵ of $(Cl)L^2Co^+$ was also taken as 67.8 M^{-1} cm^{-1}.

All the kinetic determinations were carried out as described earlier[8] by use of a laser flash photolysis system[11] and the LD 490 dye (Exciton). Most of the measurements were done at 360 nm, where the signal to noise ratio was the best. The temperature was controlled in all the experiments at 25.0 ± 0.2 °C. The concentration of O_2 was varied by combining aqueous solutions saturated with O_2, air, and argon. The solubility of O_2 in H_2O was taken as 1.28 mM[12] and in 1.0 M NaCl as 0.93 mM. The latter value was obtained by averaging all the literature data.[12b]

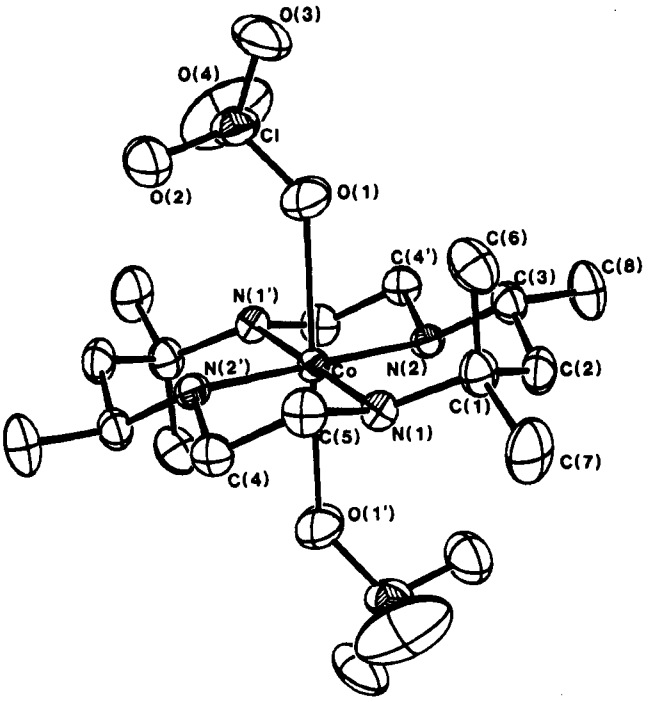

Figure 1. Structure of the complex [Co(*C-meso*-Me_6[14]aneN_4)(ClO_4)$_2$] and the numbering scheme. Ellipsoids were drawn with 50% probability.

Table II. Bond Distances (Å) for [Co(*C-meso*-Me_6[14]aneN_4)(ClO_4)$_2$]

Co–O(1)	2.408 (2)	N(2)–C(3)	1.495 (3)
Co–N(1)	2.014 (2)	N(2)–C(4')	1.487 (3)
Co–N(2)	1.997 (2)	C(1)–C(2)	1.528 (3)
Cl–O(1)	1.443 (2)	C(1)–C(6)	1.527 (4)
Cl–O(2)	1.418 (2)	C(1)–C(7)	1.535 (4)
Cl–O(3)	1.414 (2)	C(2)–C(3)	1.519 (4)
Cl–O(4)	1.428 (3)	C(3)–C(8)	1.533 (3)
N(1)–C(1)	1.512 (3)	C(4)–C(5)	1.506 (4)
N(1)–C(5)	1.484 (3)		

A single crystal of $L^2Co(ClO_4)_2$ for crystal structure analysis was obtained by passing dry argon over the surface of a solution containing 0.3 mM trifluoromethanesulfonate salt of the complex and 0.1 M $LiClO_4$. Diffraction data[13] were collected by use of an Enraf-Nonius CAD4 instrument. The cell constants were determined from a list of reflections found by an automated search routine. Pertinent data collection and reduction information is given in Table I.

A total of 4089 reflections were collected in the $\pm h,+k,\pm l$ hemisphere, of which 2050 were unique and not systematically absent. The agreement factors for the averaging of 3245 observed data were 2.6% on the basis of intensity and 1.8% on the basis of F_{obs}. The intensities of three standards, checked hourly over the course of the data collection, indicated only random variations within the errors of the measurement. Lorentz and polarization corrections were applied. A series of ψ scans indicated no significant variation in intensity with ψ, so no absorption correction was applied.

The monoclinic space group $P2_1/n$ was indicated unambiguously by the systematic absences. The Co atom was placed at the origin on the basis of the Patterson map. The remainder of the non-hydrogen atoms were located by subsequent structure factor calculations and electron density maps. Following anisotropic refinement of all of the non-hydrogen atoms, the positions of the hydrogen atoms were located in a difference map. All hydrogen atoms were then placed in idealized positions for structure factor calculations but not refined. Hydrogen temperature factors were set equal to 1.3 times the isotropic equivalent of the attached carbon atoms.

Calculations were performed on a Digital Equipment Corp. Micro VAX II computer using the CAD4-SDP programs.[14]

(11) (a) Melton, J. D.; Espenson, J. H.; Bakac, A. *Inorg. Chem.* **1986**, *25*, 4104. (b) Hoselton, M. A.; Lin, C.-T.; Schwartz, H. A.; Sutin, N. *J. Am. Chem. Soc.* **1978**, *100*, 2383. The energy of the laser pulse is 250 mJ, and the pulse width is 600 ns.

(12) (a) Benson, B. B.; Krause, D.; Peterson, M. A. *J. Solution Chem.* **1979**, *8*, 655. (b) *Solubility Data Series, Volume 7, Oxygen and Ozone*; Battino, R., Ed.; Pergamon Press: Oxford, England, 1981.

(13) The data collection and refinement were carried out at the Iowa State Molecular Structure Laboratory by Dr. L. Daniels.

(14) *Enraf-Nonius Structure Determination Package*; Enraf-Nonius: Delft, Holland.

Table III. Bond Angles (deg) in [Co(*C-meso*-Me_6[14]aneN$_4$)(ClO_4)$_2$]

O(1)-Co-O(1')	180.0 (0)	Co-N(1)-C(5)	106.9 (1)
O(1)-Co-N(1)	93.87 (8)	C(1)-N(1)-C(5)	113.7 (2)
O(1)-Co-N(1')	86.13 (8)	N(1)-C(1)-C(2)	108.1 (2)
O(1)-Co-N(2)	90.36 (8)	N(1)-C(1)-C(6)	111.0 (2)
O(1)-Co-N(2')	89.64 (8)	N(2')-C(4)-C(5)	106.8 (2)
N(1)-Co-N(1')	180.0 (0)	N(1)-C(5)-C(4)	107.2 (2)
N(1)-Co-N(2)	94.25 (8)	Co-N(2)-C(3)	118.0 (1)
N(1)-Co-N(2')	85.75 (8)	Co-N(2)-C(4')	107.2 (1)
N(2)-Co-N(2')	180.0 (0)	C(3)-N(2)-C(4')	112.8 (2)
O(1)-Cl-O(2)	108.5 (1)	N(1)-C(1)-C(7)	109.1 (2)
O(1)-Cl-O(3)	109.2 (1)	C(2)-C(1)-C(6)	111.5 (2)
O(1)-Cl-O(4)	106.5 (2)	C(2)-C(1)-C(7)	107.0 (2)
O(2)-Cl-O(3)	110.1 (1)	C(6)-C(1)-C(7)	110.0 (2)
O(2)-Cl-O(4)	109.4 (2)	C(1)-C(2)-C(3)	117.9 (2)
O(3)-Cl-O(4)	113.0 (2)	N(2)-C(3)-C(2)	109.3 (2)
Co-O(1)-Cl	133.8 (1)	N(2)-C(3)-C(8)	111.7 (2)
Co-N(1)-C(1)	124.0 (1)	C(2)-C(3)-C(8)	109.6 (2)

Table IV. Positional Parameters for [Co(*C-meso*-Me_6[14]aneN$_4$)(ClO_4)$_2$][a]

atom	*x*	*y*	*z*	*B*, Å^2
Co	0.000	0.000	0.500	1.686 (7)
Cl	0.36388 (7)	-0.20350 (8)	0.54051 (5)	3.34 (1)
O(1)	0.2493 (2)	-0.1021 (3)	0.5688 (2)	4.27 (5)
O(2)	0.4017 (3)	-0.1577 (3)	0.4575 (2)	5.07 (5)
O(3)	0.5040 (3)	-0.2043 (4)	0.6023 (2)	6.74 (7)
O(4)	0.2858 (4)	-0.3424 (3)	0.5318 (3)	9.3 (1)
N(1)	0.0528 (2)	0.2033 (2)	0.5449 (1)	2.05 (4)
N(2)	-0.1078 (2)	-0.0576 (2)	0.6031 (1)	1.95 (4)
C(1)	0.0846 (3)	0.2427 (3)	0.6410 (2)	2.55 (5)
C(2)	-0.0420 (3)	0.1669 (3)	0.6881 (2)	2.76 (5)
C(3)	-0.0413 (3)	0.0009 (3)	0.6911 (2)	2.45 (5)
C(4)	0.1215 (3)	0.2197 (3)	0.3981 (2)	2.37 (5)
C(5)	0.1732 (3)	0.2635 (3)	0.4919 (2)	2.59 (5)
C(6)	0.2545 (4)	0.1989 (4)	0.6799 (2)	3.56 (6)
C(7)	0.0613 (4)	0.4079 (3)	0.6513 (2)	4.14 (7)
C(8)	-0.1384 (4)	-0.0518 (4)	0.7630 (2)	3.98 (6)

[a] *B* values for anisotropically refined atoms are given in the form of the isotropic equivalent displacement parameter defined as $(4/3)[a^2B(1,1) + b^2B(2,2) + c^2B(3,3) + ab(\cos\alpha)B(1,2) + ac(\cos\beta)B(1,3) + bc(\cos\alpha)B(2,3)]$.

Results and Discussion

X-ray Crystal Structure of [Co(*meso*-Me_6[14]aneN$_4$)(ClO_4)$_2$]. The structure of the complex is shown in Figure 1. The cobalt atom is located at the crystallographic center of inversion, which coincides with the center of the equatorial plane containing the four nitrogens. The two remaining positions are occupied by perchlorate anions. The bond distances, bond angles, and positional parameters are given in Tables II–IV. The bond distances and bond angles within the macrocyclic ligand are quite similar to those found in analogous complexes of this ligand with other metals.[15,16]

The structure of the [Co(*meso*-Me_6[14]aneN$_4$)(ClO_4)$_2$] closely parallels that of [Co([14]aneN$_4$)(ClO_4)$_2$].[17] Both are centrosymmetric with a 1*R*,4*R*,8*S*,11*S*-stereochemistry around the nitrogens. The Co–O distances (2.409 vs 2.408 Å) are also nearly identical in the two complexes. The failure of the steric crowding in the *meso*-Me_6[14]aneN$_4$ complex to affect the cobalt–perchlorate distance probably just reflects the fact that the perchlorates are weakly bound in both complexes. The cobalt–nitrogen bonds are somewhat longer for the hexamethyl derivative (2.014 and 1.997 Å) than for the [14]aneN$_4$ complex (1.982 and 1.978 Å), indicating that the cobalt(III) state is more destabilized relative to cobalt(II) for the hexamethyl complex. This conclusion

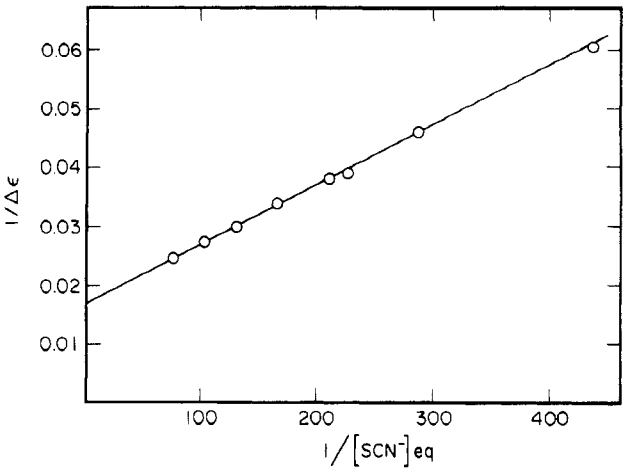

Figure 2. Plot of $1/\Delta\epsilon$ vs $1/[SCN^-]_{eq}$, suggested by eq 4 for determination of the equilibrium constant K_3 at 0.1 M ionic strength.

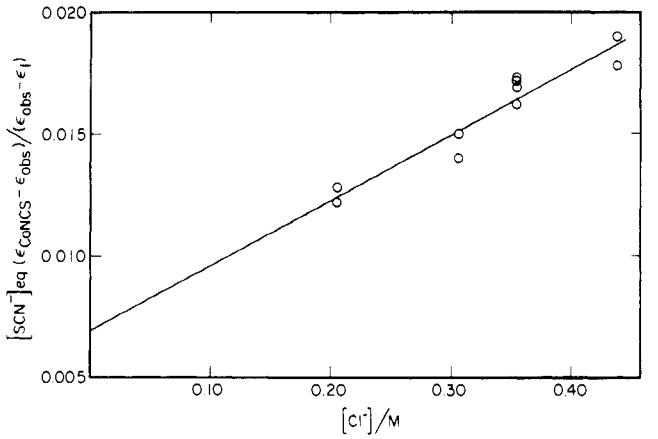

Figure 3. Plot according to eq 6 for determination of the equilibrium constant K_5 by competition between Cl^- and SCN^- for L^2Co^{2+} (L^2 = *C-meso*-Me_6[14]aneN$_4$) at 0.50 M ionic strength.

is also supported by the values of reduction potentials for the two couples.[8]

General Observations. Laser flash photolysis of solutions containing L^2Co^{2+}, O_2, and X^- (X = Cl, SCN) results in partial bleaching of the 360-nm absorbance, followed by a process that brings the absorbance back to precisely the same value it had before the flash. Identical observations were made earlier on solutions that contained no coordinating anions,[8] where it was established that $L^2CoO_2^{2+}$ photodissociates to L^2Co^{2+} and O_2 (eq 7). No absorbance changes were observed in the absence of O_2.

$$L^2CoO_2^{2+} \xrightarrow{h\nu} L^2Co^{2+} + O_2 \qquad (7)$$

Solutions of L^2Co^{2+}, X^-, and O_2 have four cobalt-containing species at equilibrium, L^2Co^{2+}, $L^2CoO_2^{2+}$, $(X)L^2Co^+$, and $(X)L^2CoO_2^+$. The photochemistry of this system could be quite complicated, since both $L^2CoO_2^{2+}$ and $(X)L^2CoO_2^+$ (eq 8) may

$$(X)L^2CoO_2^+ \xrightarrow{h\nu} (X)L^2Co^+ + O_2 \qquad (8)$$

undergo cleavage of the Co–O bond. In addition, the photolysis might induce dissociation of the ligand X^- from $(X)L^2Co^+$ and $(X)L^2CoO_2^+$. The lack of an observable absorbance change at 360 nm upon flashing an argon-saturated solution of $(SCN)L^2Co^+$ suggests, but does not prove, that no photoreaction occurs, since the molar absorptivities of both $(SCN)L^2Co^+$ and L^2Co^{2+} are small (ϵ 60 and 20 M^{-1} cm^{-1}, respectively). However, for a successful data treatment it is not necessary to know exactly which species, in addition to $L^2CoO_2^{2+}$, are photoactive, since all the equilibria in the system have to be reestablished after the flash, irrespective of the number of species cleaved in the flash.

Equilibria. The equilibrium constant for the reaction of L^2Co^{2+} with SCN^- (eq 3) was determined at 0.10 M ionic strength, as

(15) (a) Clay, R.; Murray-Rust, J.; Murray-Rust, P. *J. Chem. Soc., Dalton Trans.* **1979**, 1135. (b) Bharadwaj, P. K.; Potenza, J. A.; Schugar, H. J. *Inorg. Chem.* **1988**, *27*, 3172.
(16) Mertes, K. B. *Inorg. Chem.* **1978**, *17*, 49.
(17) Endicott, J. F.; Lilie, J.; Kuszaj, J. M.; Ramaswamy, B. S.; Schmonsees, W. G.; Simic, M. G.; Glick, M. D.; Rillema, D. P. *J. Am. Chem. Soc.* **1977**, *99*, 429.

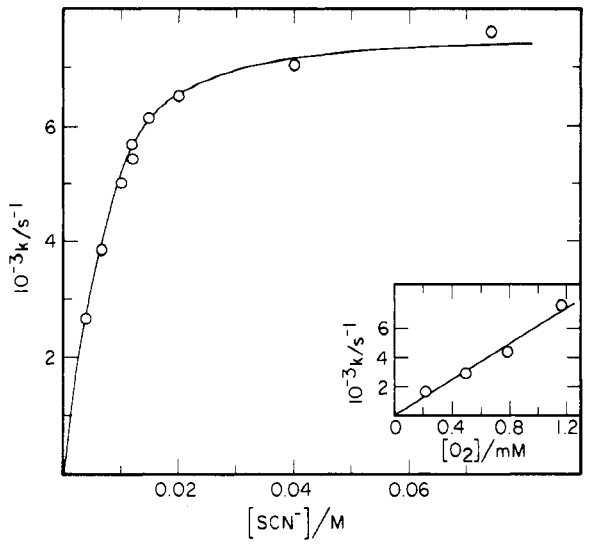

Figure 4. Plot depicting the dependence of the pseudo-first-order rate constant for the reaction of L^2Co^{2+} (L^2 = *C-meso*-Me_6[14]aneN$_4$) with O_2 and SCN^- on $[SCN^-]$ ($[O_2]$ = 1.25 mM) and on $[O_2]$ (inset, $[SCN^-]$ = 0.0743 M) at 0.10 M ionic strength.

described in the Experimental Section. A plot according to the linearized (reciprocal) form of eq 4 is shown in Figure 2. A least-squares analysis of the data according to eq 4 yielded K_3 = 174 ± 3 M^{-1}, and $\Delta\epsilon_0$ = 58.6 ± 0.6 M^{-1} cm^{-1} at 490 nm. Since ϵ = 67.8 M^{-1} cm^{-1} for L^2Co^{2+}, we obtain ϵ = 126 M^{-1} cm^{-1} for $(SCN)L^2Co^+$.

A plot according to eq 6 is shown in Figure 3. Note that the ionic strength was adjusted to 0.50 M owing to the large concentrations of Cl^- needed in these experiments. From the intercept and slope of the plot we obtain K_3 = 144 ± 18 M^{-1} and K_5/K_3 = 0.0267 ± 0.0027, and thus K_5 = 3.8 ± 0.9 M^{-1}. The value of K_3 obtained here at 0.50 M ionic strength is in reasonable agreement with the value of 174 M^{-1}, determined directly at 0.10 M ionic strength.[18] This agreement further justified our competition method for the determination of K_5.

Kinetics of the L^2Co^{2+}–O_2–SCN^- Reaction. In all the experiments the concentrations of SCN^- (4–74 mM) and O_2 (0.25–1.26 mM) were much higher than that of L^2Co^{2+} (30–60 μM), and the ionic strength was kept constant at 0.10 M. Most solutions had a natural pH (~7). In one case the rate constant was determined at pH 2. The value was within the error identical with that obtained at pH 7, but the subsequent decomposition steps were much faster at pH 2.

The increase in absorbance after the flash followed first-order kinetics well if the ratio $[SCN^-]/[O_2]$ exceeded ~20. Under those conditions the dependence of the pseudo-first-order rate constant on $[O_2]$ at constant $[SCN^-]$ is linear, but the dependence on $[SCN^-]$ at constant $[O_2]$ reaches saturation at $[SCN^-] \geq 30$ mM. The data are shown in Figure 4.

In the experiments that had the ratio $[SCN^-]/[O_2]$ significantly less than 20, the reaction appeared to have a rapid initial stage followed by a slower, pseudo-first-order process. The size of the signal in the initial stage and the time scale of the reaction identify it as the known[8] equilibration process of eq 9. The kinetic and

$$L^2Co^{2+} + O_2 \rightleftarrows L^2CoO_2^{2+} \qquad K = 301\ M^{-1} \qquad (9)$$

thermodynamic parameters involved in the complete reaction scheme, see later, as well as the molar absorptivities of all the species involved are such that reaction 9 can be observed as a separate step only under the conditions that are most favorable for the formation of $L^2CoO_2^{2+}$, i.e. high $[O_2]$, and least favorable for the formation of the thiocyanate adduct, i.e. low $[SCN^-]$. The

(18) The equilibrium constant K_3 could not be determined directly, i.e. in the absence of chloride, at 0.5 M ionic strength owing to the low solubility of both L^2Co^{2+} and $(SCN)L^2Co^+$ in solutions containing high concentrations of ClO_4^-.

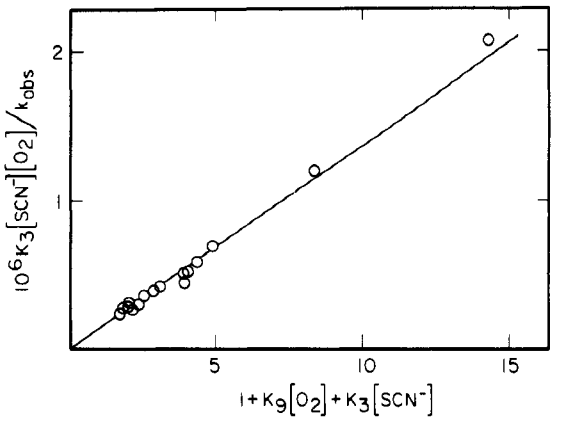

Figure 5. Plot according to eq 12 for the reaction of L^2Co^{2+} (L^2 = *C-meso*-Me_6[14]aneN$_4$) with O_2 and SCN^-.

Table V. Summary of the Kinetic Data for the Autoxidation of L^2Co^{2+} (L^2 = *C-meso*-Me_6[14]aneN$_4$) in the Presence and Absence of Cl^- in O_2-Saturated Solutions[a]

$[Cl^-]$/M	$10^{-4}k_{fast}$/ s^{-1}	$10^{-3}k_{slow}$/ s^{-1}	$[Cl^-]$/M	$10^{-4}k_{fast}$/ s^{-1}	$10^{-3}k_{slow}$/ s^{-1}
0	2.4[b]		0.50		5.1[b]
0.024	2.3	3.8	0.50[c]		5.1[b]
0.10	2.9	4.4	1.0		5.1[b]
0.20[c]	2.4	4.1			

[a] 25 °C, $[L^2Co^{2+}]_0$ = 0.2 mM, pH 1.3–7. $[O_2]$ varies somewhat in these experiments owing to the lower solubility in 1 M NaCl (0.94 mM) and 1 M $LiClO_4$ (1.10 mM) than in pure H_2O (1.28 mM); see text. [b] Single-stage reaction. [c] μ = 1.0 M ($LiClO_4$ + NaCl).

rate constant for the subsequent slower reaction of interest was determined by successively removing points from the beginning of the trace until further removal of points had no effect on the rate constant. Even under the least favorable conditions employed, it sufficed to remove the initial 10–15% of the reaction.

A reaction scheme that satisfactorily explains all the observations is given by eqs 3, 9, and 10. The kinetics of the formation

$$(SCN)L^2Co^+ + O_2 \rightarrow (SCN)L^2CoO_2^+ \qquad (10)$$

of the product $(SCN)L^2CoO_2^+$ are given by eq 11, which upon rearrangement gives eq 12. The term $[L^2Co^{II}]_t$ represents the

$$d[(SCN)L^2CoO_2^+]/dt = \frac{k_{10}K_3[O_2][SCN^-][L^2Co^{II}]_t}{1 + K_9[O_2] + K_3[SCN^-]} = k_{obs}[L^2Co^{II}]_t \qquad (11)$$

$$K_3[SCN^-][O_2]/k_{obs} = (1 + K_9[O_2] + K_3[SCN^-])/k_{10} \qquad (12)$$

total concentration of cobalt(II). The least-squares fit of the data to eq 11 yields k_{10} = (7.29 ± 0.14) × 10^6 M^{-1} s^{-1}. The values of K_3 (174 M^{-1}) and K_9 (301 M^{-1}) were fixed in this calculation. A plot according to eq 12 is shown in Figure 5.

The UV–visible spectrum of $(SCN)L^2CoO_2^+$ was obtained in the presence of an excess of O_2 and SCN^-, such that no other cobalt-containing species existed in solution in significant amounts. The spectrum exhibits maxima at 465 nm (ϵ 520 M^{-1} cm^{-1}) and 315 nm (ϵ (7.4 × 10^3 M^{-1} cm^{-1}).

The equilibrium of eq 9 is known to be rapid and, more importantly, shifted to the left.[8] Under the experimental conditions in this work the amount of $L^2CoO_2^{2+}$ at equilibrium never exceeded 15% of the total cobalt. The effect of eq 9 on the overall kinetics is thus minor, although not negligible. The value of the rate constant k_{-9} is 1.66 × 10^4 s^{-1}, which is sufficient, although barely so, to qualify as "rapid" compared to >6 × 10^3 s^{-1}. The latter is the value of the term $k_{10}K_3[O_2][SCN^-]/(1 + K_3[SCN^-])$ under the conditions of low $[SCN^-]$, where kinetically significant amounts of $L^2CoO_2^{2+}$ (>5% of total cobalt) exist in solution. Kinetic data are not available for reaction 3, although the good fit of the data to eq 11 serves as evidence that the equilibrium is indeed rapid, as expected, on the time scale of reaction 10.

Table VI. Summary of the Kinetic and Equilibrium Data for the Reactions of L^2Co^{2+} (L^2 = *C-meso*-Me_6[14]aneN$_4$) with O_2, Cl^-, and SCN^- at 25 °C

reacn	$10^{-2}K$/M	$10^{-6}k_f$/M^{-1} s^{-1}	$10^{-4}k_r$/s^{-1}
$L^2Co^{2+} + O_2 \rightleftharpoons L^2CoO_2^{2+}$ [a,b]	3.01 (40)	5.00 (47)	1.66 (5)
$(Cl)L^2Co^+ + O_2 \rightleftharpoons (Cl)L^2CoO_2^+$ [c]	5.60 (120)	1.80 (26)	0.321 (20)
$(SCN)L^2Co^+ + O_2 \rightleftharpoons (SCN)L^2CoO_2^+$ [d]	>150	7.29 (14)	<0.05[e]
$L^2Co^{2+} + Cl^- \rightleftharpoons (Cl)L^2Co^+$ [f]	0.038 (9)		
$L^2Co^2 + SCN^- \rightleftharpoons (SCN)L^2Co^+$ [d]	1.74 (3)		

[a] Reference 8. [b] μ = 0.001–1.0 M ($LiClO_4$). [c] In 1.0 M NaCl. [d] μ = 0.10 M ($LiClO_4$ + LiSCN). [e] Reaction not observed. [f] μ = 0.50 M ($LiClO_4$ + NaCl).

Another scheme, that is kinetically indistinguishable from the proposed one, would have $L^2CoO_2^{2+}$ react with SCN^- in the rate-determining step (eq 13), and some of the cobalt would now

$$L^2CoO_2^{2+} + SCN^- \rightarrow (SCN)L^2CoO_2^+ \qquad (13)$$

be stored as the unreactive $(SCN)L^2Co^+$. This proposal cannot be completely ruled out, and it is possible that both pathways, eqs 10 and 13, contribute, in which case the complete rate law is given in eq 14. The value of the numerator is 1.27×10^9 M^{-2}

$$k_{obs} = \frac{k_{10}K_3 + k_{13}K_9}{1 + K_3[SCN^-] + K_9[O_2]}[SCN^-][O_2] \qquad (14)$$

s^{-1}. In the analysis that neglected reaction 13 this value was assigned to the product $k_{10}K_3$.

The available evidence suggests that reaction 13 is not a major pathway. If it were, the proposed scheme would break down at high $[SCN^-]$ because the formation of $L^2CoO_2^{2+}$ by the sequence eqs −3 and 9 would become rate-determining. For example, in an experiment having 0.074 M SCN^-, 0.22 mM O_2, and 36 μM total cobalt, the observed rate constant was 1.55×10^3 s^{-1} and yet the calculated value of the supposedly fast preequilibrium term $k_9[O_2]/(1 + K_3[SCN^-])$ is only 79 s^{-1}. Thus, at least at high $[SCN^-]$, $L^2CoO_2^{2+}$ is not kinetically important. At the other extreme, i.e. at low $[SCN^-]$ and high $[O_2]$, some contribution from reaction 13 is possible, although once again a good fit of *all* the data to eq 11 requires that the major portion of the reaction not involve eq 13. In a study of autooxidation of a different cobalt(II) macrocycle in the presence of halides, Dreos et al. have also concluded that the reaction of the oxygen adduct with X^- was kinetically unimportant.[3]

Kinetics of the L^2Co^{2+}–O_2–Cl^- Reaction. At high concentrations of Cl^- (>0.5 M) the kinetics are independent of $[Cl^-]$ and the rate law of eq 15 applies (Figure 6). The equilibrium concentrations

$$k_{obs} = k_f\{[L^2Co^{II}]_{eq} + [O_2]_{eq}\} + k_r \qquad (15)$$

of L^2Co^{II}, which is present mainly as $(Cl)L^2Co^+$, and of O_2 were calculated from the total concentrations by use of an initially estimated $K = k_f/k_r \sim 400$ M^{-1}. The data in Figure 6 yield $k_f = (1.80 \pm 0.26) \times 10^6$ M^{-1} s^{-1} and $k_r = (3.21 \pm 0.20) \times 10^3$ s^{-1}, and from the ratio $K = 560 \pm 120$ M^{-1}.

The form of the rate law 15 is identical with that obtained in the absence of Cl^-,[8] but the values of the rate constants are different. For comparison Figure 6 also displays the results for $[Cl^-] = 0$. Those have been shown to be independent of ionic strength in the range 0.001–1.0 M.

At intermediate concentrations of Cl^- (0.02–0.2 M) a two-stage reaction is observed. The two stages were resolved graphically by a standard procedure applicable to a series of two consecutive or independent parallel first-order reactions. The fit of the data is acceptable, although the scatter is rather large owing to the small signal to noise ratio in the later stages of the reaction. The pseudo-first-order rate constants for both stages are independent of $[Cl^-]$, but the size of the absorbance change in the slow stage increases and in the fast stage decreases as $[Cl^-]$ increases. A summary of the pertinent kinetic data in Table V for O_2-saturated solutions shows that the rate constant for the fast stage agrees well with that obtained in the absence of Cl^-; the slow stage takes place with a rate constant that is quite similar to that observed directly in single-stage reactions at high $[Cl^-]$.[19] All the rate constants in Table V are independent of ionic strength and the pH in the range 1.3–7.

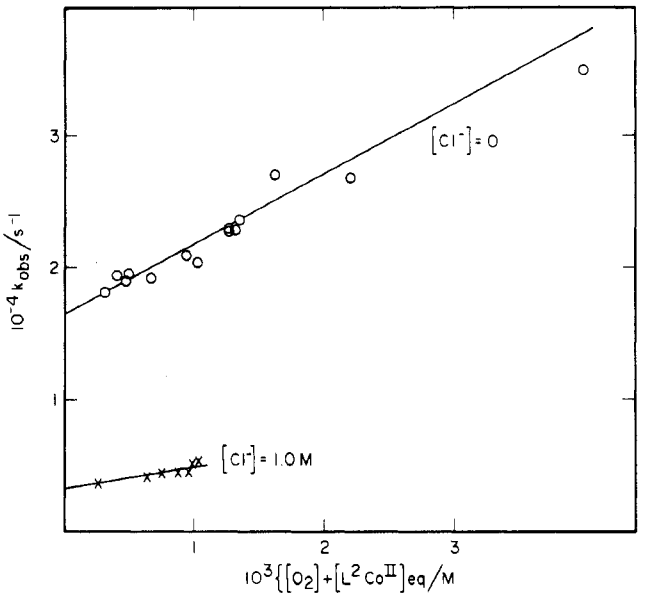

Figure 6. Plot according to eq 15 for the reaction of L^2Co^{2+} (L^2 = *C-meso*-Me_6[14]aneN$_4$) with O_2 in the presence and absence of Cl^-.

The data are consistent with a scheme whereby the products are formed in two parallel reactions (eqs 9 and 16) from the rapidly equilibrated mixture of L^2Co^{2+} and $(Cl)L^2Co^+$ (eq 5). Reaction

$$(Cl)L^2Co^+ + O_2 \rightleftharpoons (Cl)L^2CoO_2^+ \qquad (16)$$

9 is not a rapid preequilibrium step in the formation of $(Cl)L^2CoO_2^+$ but represents an independent kinetic route to the other reaction product, $L^2CoO_2^{2+}$. The difference in the kinetic behavior between the chloride and thiocyanate systems is caused mainly by the large difference in equilibrium constants K_{10} and K_{16}.

According to the proposed scheme both kinetic paths should be chloride dependent, contrary to our observations. The lack of an appreciable effect of $[Cl^-]$ on k_{obs} arises from the reverse terms, k_{-9} and k_{-16}, in the overall kinetics. Our calculations show that at intermediate concentrations of Cl^- the values of k_{obs} for the two paths should be within 10% of their limiting values in Figure 6. The effect should be more pronounced at the concentration extremes, but by then the absorbance changes for the affected terms become too small to be observed as independent stages.

Originally we set out to answer the following question: what is the exact function of X^- in the autoxidation of L^2Co^{2+}? Specifically we wanted to find out whether X^- affects mainly the kinetics and/or equilibrium parameters for the binding of O_2 or whether it only facilitates subsequent redox steps. As it turns out, the two anions studied in this work act in different ways. Thio-

(19) The concentration of O_2 in Table I varies from 0.94 mM (1.0 M NaCl) to 1.28 mM (no electrolyte added) owing to the decreased solubility of O_2 in the presence of NaCl and $LiClO_4$.[12] However, this variation is too small to have a significant effect on the rate constants, since the dominant kinetic term of eq 15 shows no dependence on $[O_2]$; see Figure 6.

cyanate has a pronounced effect on the oxygen binding step, and chloride effects mainly the subsequent redox steps.

The rate constant for the binding of O_2 is fairly insensitive to the presence of anions. The values of k_f for the three species in Table VI differ only by a factor of ~4. This is somewhat surprising, since one might have expected that differences in oxygen affinity would be reflected in the kinetics of both forward and reverse reactions.

The effect on the release of O_2 is much more pronounced. The rate constant k_r is the largest for the aquo complex, intermediate for the chloro, and too small to observe for the thiocyanato. The electronic structure of these cobalt-oxygen adducts is probably best considered intermediate between $Co^{II}-O_2$ and $Co^{III}-O_2^-$.[1e,5] The latter structure should be stabilized the most by the most strongly coordinated anion, SCN^-, and thus the dissociation to O_2 and cobalt(II) should be least favorable for $(SCN)L^2CoO_2^+$, as experimentally observed. The high equilibrium constant for the binding of O_2 might be partly responsible for the accelerated autoxidation of L^2Co^{2+} in the presence of SCN^-. Subsequent redox steps were not investigated, but they are probably affected too, as judged from the results obtained in the presence of chloride.

The equilibrium constant for the binding of O_2 by $(Cl)L^2Co^+$, 560 M^{-1}, is not much larger than that for the uncomplexed L^2Co^{2+}, 301 M^{-1}. Both the forward and reverse reactions are somewhat faster for L^2Co^{2+} than for $(Cl)L^2Co^+$. Despite that, the irreversible oxidation of L^2Co^{2+} is much faster in the presence of Cl^-, demonstrating that the redox steps following reaction 16 must be accelerated by Cl^-. Similar conclusions have been reached earlier for some other cobalt complexes.[3,4] We have also observed that Br^- accelerates dramatically the autoxidation of L^2Co^{2+}, although it has no effect on the oxygen binding step. This is also consistent with strong catalysis in the redox steps. A detailed study of these reactions is in progress.

Acknowledgment. This research was supported by the U.S. Department of Energy, Office of Basic Energy Sciences, Chemical Sciences Division, under Contract W-7405-Eng-82. We are grateful to S. Lee for the synthesis of the macrocyclic ligand and to Dr. Lee Daniels of the Iowa State University Molecular Structure Laboratory for the crystal structure determination.

Registry No. $(Cl^-)L^2Co^+$, 126543-76-8; $(SCN^-)L_2Co^+$, 126543-77-9; $[Co(C\text{-}meso\text{-}Me_6[14]aneN_4)(ClO_4)_2]$, 126543-78-0.

Supplementary Material Available: Tables of positional parameters for hydrogen atoms and general displacement parameter expressions (5 pages); a listing of observed and calculated structure factors (8 pages). Ordering information is given on any current masthead page.

Contribution from the Department of Chemistry, Stanford University, Stanford, California 94305

Variable-Energy Photoelectron Spectroscopic Comparison of the Bonding in Ferric Sulfide and Ferric Chloride: An Alternative Description of the Near-IR-Visible Spin-Forbidden Transitions in High-Spin d^5 Complexes

Kristine D. Butcher, Matthew S. Gebhard, and Edward I. Solomon*

Received September 25, 1989

Variable photon energy, valence-band, and core-level photoelectron spectroscopy (PES) have been used to determine the electronic structure and bonding in tetrahedral high-spin d^5 FeS_4^{5-}. The valence-band PES spectra over the range 25-100 eV show strong similarities with our previous results on tetrahedral $FeCl_4^-$. The three-peak pattern and their energy splittings and intensity ratios all parallel the data on $FeCl_4^-$. Also, as in ferric chloride, the major resonance enhancement appears in the deepest binding energy portion of the main band, indicating that dominant metal character is present in the bonding levels at deepest binding energy. No off-resonance PES intensity is observed in the satellite, indicating that little relaxation occurs upon ionization. These results demonstrate that the ground-state electronic structure of ferric sulfide parallels that of ferric chloride and is inverted from the normal description for transition-metal complexes, which places the dominant metal character in the antibonding levels at lowest binding energy. This inverted bonding scheme results from the large spin-polarization effects present in high-spin d^5 complexes. Analysis of the Fe 2p core level PES spectra allows a comparison of the covalency of tetrahedral ferric chloride and sulfide. The difference is relatively small and is due to the lower ionization energy of the sulfide relative to the chloride ligands. Alternatively, there is a large difference observed between the bound-state optical absorption spectra of ferric chloride relative to the sulfide (and thiolate) complex, which is not satisfactorily accounted for by ligand field theory but is explained by spin-unrestricted $X\alpha$ calculations. These studies indicate that the lowest energy spin-forbidden transitions in high-spin d^5 complexes, which are normally described as $d \rightarrow d$ transitions in ligand field theory, have extensive ligand-to-metal charge-transfer character.

I. Introduction

Our previous work has focused on determining the electronic structure and bonding in high-spin tetrahedral ferric chlorides as a first step toward understanding iron-sulfur active sites in proteins such as rubredoxin.[1] Theoretical studies of model iron thiolate complexes indicate that the ground-state bonding description of these iron-sulfur systems is inverted, with the HOMO exhibiting mostly ligand character and the metal character contained in the bonding levels at deeper binding energy.[2] This inverted ground state is also predicted for $FeCl_4^-$ and was experimentally confirmed by using variable-energy photoelectron spectroscopy (PES).[1d] The energy level diagram for the high-spin d^5 system including exchange can be depicted schematically as in Figure 1. The ground-state spin-unrestricted $X\alpha$ calculations indicate that the stabilization of the d levels is due to the large exchange interaction in high-spin d^5, which lowers the energy of the occupied $d\uparrow$ orbitals relative to the empty $d\downarrow$ orbitals.[3] The exchange splitting between ligand $\uparrow$ and $\downarrow$ levels is small, while the exchange in the Fe 3d levels is large and is present in the free-ion ^6S ground state. This exchange splitting is the greatest for the d^5 configuration and is sufficient to drop the $3d\uparrow$ levels below the ligand 3p valence levels. Both the $d\uparrow$ and $d\downarrow$ orbitals interact with the ligand 3p valence orbitals, resulting in a complex bonding scheme that contains dominant ligand character in both the spin-down bonding and

(1) (a) Deaton, J. C.; Gebhard, M. S.; Koch, S. A.; Millar, M.; Solomon, E. I. *J. Am. Chem. Soc.* **1988**, *110*, 6241. (b) Gebhard, M. S.; Deaton, J. C.; Koch, S. A.; Millar, M.; Solomon, E. I. *J. Am. Chem. Soc.*, in press. (c) Deaton, J. C.; Gebhard, M. S.; Solomon, E. I. *Inorg. Chem.* **1989**, *28*, 877. (d) Butcher, K. D.; Didziulis, S. V.; Briat, B.; Solomon, E. I. *J. Am. Chem. Soc.*, in press.

(2) (a) Norman, J. G., Jr.; Jackels, S. C. *J. Am. Chem. Soc.* **1975**, *97*, 3833. (b) Norman, J. G., Jr.; Ryan, P. B.; Noodleman, L. *J. Am. Chem. Soc.* **1980**, *102*, 4279. (c) Bair, R. A.; Goddard, W. A., III. *J. Am. Chem. Soc.* **1978**, *100*, 5669.

(3) The spin-unrestricted formalism allows different orbitals for different spins, thus splitting the d orbitals into occupied spin-up and unoccupied spin-down.

0020-1669/90/1329-2067$02.50/0 © 1990 American Chemical Society